Graph convolution based residual connected network for morphological reconstruction in fluorescence molecular tomography

Wang, Yu, Bian, Chang, An, Yu, Wang, Hanfan, Liang, Qian, et al.

Yu Wang, Chang Bian, Yu An, Hanfan Wang, Qian Liang, Yang Du, Jie Tian, "Graph convolution based residual connected network for morphological reconstruction in fluorescence molecular tomography," Proc. SPIE 12036, Medical Imaging 2022: Biomedical Applications in Molecular, Structural, and Functional Imaging, 120361X (4 April 2022); doi: 10.1117/12.2605349

SPIE.

Event: SPIE Medical Imaging, 2022, San Diego, California, United States

Graph Convolution Based Residual Connected Network for Morphological Reconstruction in Fluorescence Molecular Tomography

Yu Wang[1,2], Chang Bian[1,2], Yu An[1,3], Hanfan Wang[1,4],Qian Liang[1], Yang Du*[,1,2],Jie Tian*[,1,2,3,4]

1. CAS Key Laboratory of Molecular Imaging, the State Key Laboratory of Management and Control for Complex Systems, Institute of Automation, Chinese Academy of Sciences, Beijing, 100190, China
2. School of Artificial Intelligence, The University of Chinese Academy of Sciences, Beijing, 100049, China
3. Beijing Advanced Innovation Center for Big Data-Based Precision Medicine, School of Medicine, Beihang University, Beijing, 100191, China
4. Engineering Research Center of Molecular and Neuro Imaging of Ministry of Education, School of Life Science and Technology, Xidian University, Xi'an, Shaanxi, 710126, China

*Corresponding authors, E-mail: yang.du@ia.ac.cn, tian@ieee.org

ABSTRACT

Fluorescence molecular tomography (FMT) is a promising multimodality-fused medical imaging technique, aiming at noninvasively and dynamically visualizing the interaction processes at the cellular and molecular level. However, the quality of FMT reconstruction is limited by the simplified linear model of photon propagation. In this work, we propose a novel GCN based Residual connected (GCN-RC) network to improve the quality of FMT morphological reconstruction. Instead of using a simplified linear model of photon propagation for FMT recon-struction, the method can directly construct a nonlinear mapping relationship between the photon density of an object surface and its internal fluorescent source. GCN-RC network consists of a fully connected(FC) sub-network and a GCN sub-network connected by means of residual connection. The FC sub-network provides a coarse reconstruction result and GCN sub-network fine-tunes the morphological quality of reconstructed result. In order to validate the reconstruction performance of GCN-RC, we performed numerical simulation experiments and in vivo experiments based on tumor-bearing mice. Comparisons were performed with the L2-based Tikhonov method (Tikhonov-L2), inverse problem simulation (IPS) method and GCN-RC method. Both numerical simulated and in vivo experimental results demonstrated that GCN-RC achieved improved reconstruction in terms of both source localization and morphology recovery.

Keywords: fluorescence molecular tomography, Graph convolution network, inverse problem.

1. INTRODUCTION

Fluorescence Molecular Imaging (FMI) is a widely applied optical imaging modality for numerous biomedical applications[1, 2]. FMI provides millimeter-level spatial resolution and shows the advantages of high detection sensitivity, high signal intensity, and ease of clinical translation. In recent years, FMI has received extensive attention and becomes one of the hot topics in the field of optical molecular imaging. However, due to the severe absorption scattering problem when the photons propagate in the organism[3, 4], FMI can only locate the distribution of fluorescence source from two-dimensional space, but cannot obtain the depth information of fluorescence source inside the object. Therefore, fluorescence molecular tomography (FMT) has been proposed to perform depth reconstruction, which can fuse the tumor-specific molecular information from FMI with anatomical spatial information from Computed Tomography (CT)[5, 6].

In recent years, research on FMT has focused on improving the quality of 3D reconstruction, especially the location accuracy and morphological reconstruction accuracy. Generally, the main task of FMT is to reconstruct the distribution of an internal fluorescent sources under the condition that the distribution of its surface photon intensity is known. However, the complexity of photon propagation model and the ill-posedness of inverse problem still limit the further development of FMT reconstruction[7]. To solve the problems encountered in FMT reconstruction, researchers have proposed two reconstruction methods. The first reconstruction method is mainly based on a photon propagation model[8-11]. This method

Medical Imaging 2022: Biomedical Applications in Molecular, Structural, and Functional Imaging,
edited by Barjor S. Gimi, Andrzej Krol, Proc. of SPIE Vol. 12036, 120361X
© 2022 SPIE · 1605-7422 · doi: 10.1117/12.2605349

uses the 3D spatial information provided by CT as a priori information to build a forward model of photon propagation in an organism by means of a higher-order spherical harmonic approximation. The solution is usually carried out using a regularization-based coordinate descent algorithm. Although these methods improved the performance of FMT reconstruction, the deviation between simplified photon propagation model and actual process of light propagation still limits the accuracy of FMT reconstruction. The second reconstruction method is mainly based on machine learning[12, 13]. This method establishes the model of inverse photon propagation directly by learning the nonlinear mapping relation between the surface photon intensity and internal fluorescent source. The solution is usually carried out using multi-layer perceptron (MLP) algorithm to simulate inverse problem. However, its over-sparse problem limited the morphological reconstruction. Therefore, the morphological reconstruction of FMT based on machine learning is still an urgent challenge to be solved.

In this work, we propose a novel GCN based Residual connected (GCN-RC) network to improve the quality of FMT morphological reconstruction[14]. The method takes advantage of the structural priori feature that fluorescent sources tend to be distributed in clusters within an organism, and uses GCN to extract spatial features to optimize morphological reconstruction results. To validate the reconstruction performance of GCN-RC, we conducted numerical simulation experiments based on digital mouse and also *in vivo* experiments on tumor bearing mice.

2. METHODS

2.1 FMT inverse problem

For a steady-state FMT that has the point excitation sources, photon propagation in biological tissues can be described by the complex integral-differential radiative transfer equation[15]. Based on the finite element analysis and spherical harmonic approximation, a linear relation between the surface photon intensity and the distribution of fluorescent source inside the object can be constructed as follows:

$$\Phi = A\,X \tag{1}$$

where Φ represents the photon intensity on the object surface. A is the system matrix, and X denotes the distribution of fluorescent source inside the object. Therefore, the FMT inverse problem can be constructed as follows:

$$X = f(\Phi) \tag{2}$$

Machine learning based reconstruction methods can use the non-linear fitting capabilities of deep learning to construct mapping relationship $f(\cdot)$ between X and Φ.

2.2 Data processing of FMT

In this work, the data processing work consists of the following four sections, CT image acquisition, organ segmentation, tetrahedral meshing and dataset setup, as shown in Fig. 1. The CT imaging acquisition section was carried out on a healthy mouse to obtain mouse structural data based on the multimodal imaging system, which was developed by the key laboratory of molecular imaging of Chinese Academy of Sciences[13]. The organ segmentation section focused on intercepting parts of the brain from CT images of mice, using a combination of region-based growth and manual outlining to segment the muscle, skull and brain regions from the mouse brain. The tetrahedral meshing section used tetrahedra to approximate the distribution of mouse tissue structures. Through this approach, a standard mesh for FMT reconstruction is obtained using a tetrahedral mesh algorithm, which contains 9726 nodes and 51055 tetrahedrons.

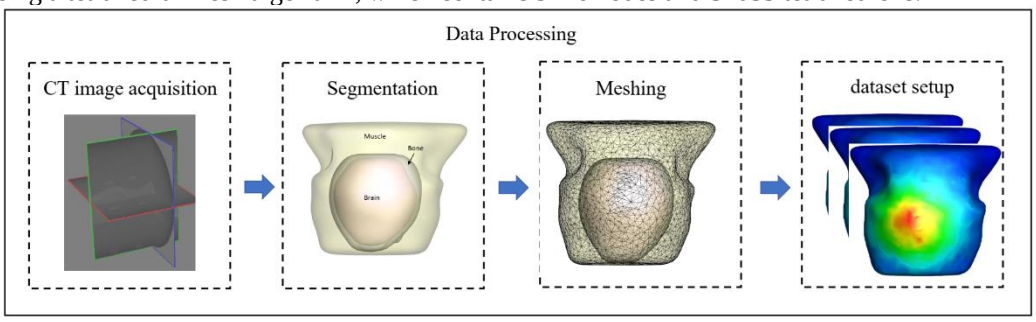

Fig. 1 four sections of data processing.

Considering that it would be impractical to collect surface photon intensities by performing thousands of *in vivo* experiments, we chose the Monte Carlo (MC) method for the collection of the dataset[16]. MC has been widely used to

simulate the photon transmission in biological tissue, which can provide both surface photon intensity and gold standard of fluorescent sources. In the dataset setup section, the collection was performed by using MOSE 2.3[17], which was developed by the key laboratory of molecular imaging of Chinese Academy of Sciences. We can obtain photon intensity by entering the standard grid, the optical coefficients of the different organs and the size and position of the fluorescence source into MOSE. The specific organ optical coefficients are listed in Table I. Finally, we employed MOSE and collected 5811 cases of FMT simulations with different positions of the single fluorescent source to build the single-source sample set, of which 900 cases were randomly selected as the test set and the rest as the training set.

TABLE I
OPTICAL PARAMETERS OF MAIN ORGANS

Organ	$\mu_{ax}\,(\mathrm{mm}^{-1})$	$\mu_{am}\,(\mathrm{mm}^{-1})$	$\mu_{sx}\,(\mathrm{mm}^{-1})$	$\mu_{sm}\,(\mathrm{mm}^{-1})$
Muscle	0.0201	0.0190	4.2735	3.7944
Bone	0.0393	0.01321	24.9193	23.4166
Brain	0.0136	0.0131	16.4450	14.4301

Furthermore, in order to improve the reconstruction accuracy and generalization ability of the model, we used data augmentation for the expansion of the dataset. Dual-source samples and big-source samples were assembled by selecting and adding the corresponding data of single-source samples. The assembled source set was calculated as follows:

$$\Phi_{ass} = \sum_{i \in S_n} \Phi_i \tag{3}$$

$$X_{ass} = \sum_{i \in S_n} X_i \tag{4}$$

where Φ_{ass} and X_{ass} represent the surface photon and the fluorescent source of assembled sample, respectively. S_n is the set of selected single-source samples and n is the number of selected samples, Φ_i and X_i represent the surface photon and the fluorescent source of i-th single-source, respectively. Dual-source samples were created by randomly selecting two samples (n=2) from the single-source samples. Big-source samples were constructed by centering on a single-source sample and assembling n nearest single-source samples (n= 2~10).

In total, we constructed 6000 assembled samples (3000 dual-source samples and 3000 big-source samples) from the single-source training sample. Similarly, we constructed 2000 assembled samples (1000 dual-source samples and 1000 big-source samples) from the single-source test sample.

2.3 GCN-RC network

The GCN-RC network proposed in this paper consists of two parts, the FC sub-network and the GCN sub-network, as shown in Fig. 2. The FC sub-network input data is the fluorescence vector Φ after max-min normalization. The FC sub-network utilized multi-layer perceptron networks to construct the mapping relation between Φ and X to locate the fluorescent source and get coarse reconstruction results. The FC sub-network consists of a four-layer fully connected network. All hidden layers are equipped with the rectification (ReLU) non-linearity and dropout (probability=20%) function to reduce the overfitting problem of the network. Besides, to speed up the convergence of the network, a maximum-minimum normalization is added between each two layers of the network.

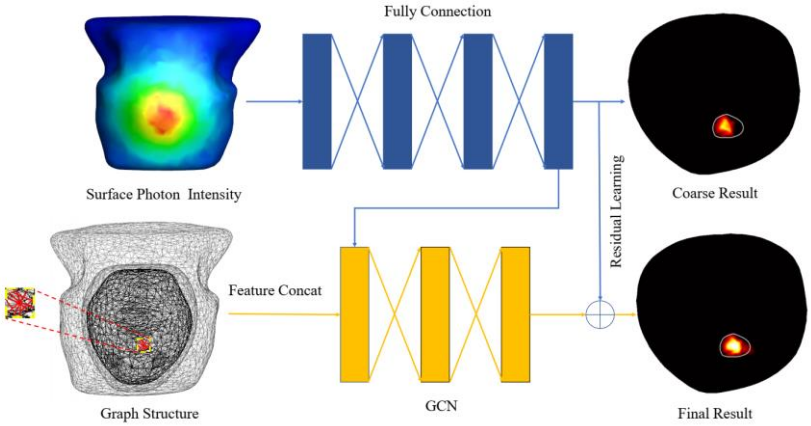

Fig. 2 Structure of GCN-RC network.

In order to overcome the over-sparse problem of FC sub-network, GCN-RC network utilized GCN sub-network to fine tune the morphological reconstruction results of FC sub-network. The GCN sub-network input data consists of two parts,

the graph weighted adjacency matrix of standard mesh and the feature vector. The nodes on the graph are the nodes of interest in the standard mesh and the edges are the edges of the tetrahedron mesh. Besides, the whole graph is undirected and weighted adjacency matrix calculated as follows:

$$w_{i,j} = \begin{cases} 1, & \text{if } i = j \\ \text{length}(p_i - p_j), & \text{if } edge_{i,j} = 1 \\ 0, & \text{if } edge_{i,j} = 0 \end{cases} \tag{5}$$

Where $w_{i,j}$ represents the edge weights between the i-th node and the j-th node, $edge_{i,j} = 1$ means there is an edge between the i-th node and the j-th node, otherwise there is no edge. In order to make full use of surface photon intensity and improve the generalization ability of the model, we encode the surface photon intensity and coarse reconstruction result into the feature vector. We define h_i^0 as the initialized feature vector of the i-th node. The initialized feature vector contains the coarse reconstruction result which represents the probability that the i-th node is part of fluorescent source, and k-nearest body surface fluorescence intensity which represents the fluorescence intensity of the k-nearest body surface nodes to the i-th node.

After obtaining feature vector h_i^0 for each node, we feed them into the GCN sub-network. The GCN sub-network consists of a three-layer GCN network. Each graph-based convolutional layer is defined as:

$$h_i^{l+1} = w_0 h_i^l + \sum_{i' \in N_i} w_1 h_{i'}^l \tag{6}$$

Where h_i^l is the feature vector attached on node i at layer l, w_0 and w_1 are learned parameter of layer l, with w_1 being shared by all edges, N_i is the neighbouring node of node i.

Ultimately, the output of the GCN-RC network is the residual value between two sub-network. The reconstruction loss is defined as follow:

$$L = \lambda \left\| X_{FC} - X_{\text{true}} \right\|_2^2 + (1-\lambda) \left\| X_{\text{final}} - X_{\text{true}} \right\|_2^2 \tag{7}$$

Where X_{FC} and X_{final} represent the output of FC sub-network and GCN-RC network, respectively. X_{true} is the ground truth. $\|X_{FC} - X_{\text{true}}\|_2^2$ and $\|X_{\text{final}} - X_{\text{true}}\|_2^2$ represent loss of positioning accuracy and loss of morphological accuracy respectively. Adjusting parameter λ can balance the ratio of the two losses.

The network was implemented by Pytorch 1.4.0 on Python 3.6.5 and trained with batch size of 64, and Adam optimizer with default parameters. The learning rate was set to 0.0001. The parameter k of k-nearest body surface nodes was set to 32. The hardware configuration of the computer is a CPU of Intel Core i7 3.4 GHz, RAM of 32GB and a GPU of GTX1080Ti.

2.4 Evaluation index

In this work, we use barycenter error (BCE), percentage of non-zero components (PNZ), and the Dice coefficient to quantitatively assess the reconstruction performance.

$$BCE = \|P_r - P_0\|_2, \quad PNZ = \frac{|X \cap Y|}{|Y|}, \quad Dice = \frac{2|X \cap Y|}{|X| + |Y|} \tag{8}$$

Where P_r and P_0 represent the reconstructed tumor centers and ground truth center, respectively, X is the confidence of reconstructed region and Y is the confidence of ground truth region. The greater value of PNZ and Dice means the better reconstruction performance, with one as the upper limitation; while the smaller BCE means the better locating performance, with the zero as the lower limitation .

3. EXPERIMENTS AND RESULTS

In order to prove the feasibility and advantage of our proposed method, numerical simulation experiments and *in vivo* mouse experiment were implemented in this section. Contrast methods including Tikhonov-L2 and IPS were utilized for comparison[11, 12].

We compared the performance of GCN-RC network with Tikhonov-L2 and IPS methods by reconstructing different samples in validation set. The performance of different methods in small-source reconstruction and big-source reconstruction were shown in TABLE II and TABLE III respectively.

Both tables showed that GCN-RC network obtained the minimum BCE maximum Dice and maximum PNZ, which proved the capability of GCN-RC network in achieving accurate source localization and morphological reconstruction. As shown in **Fig. 3**, The GCN-RC network can also achieve better reconstruction results in dual-source reconstruction.

TABLE II
QUANTITATIVE RESULTS (MEAN) OF SMALL-SOURCE RECONSTRUCTION IN VALIDATION SET

Method	Tikhonov-L2	IPS	GCN-RC
BCE(mm)	0.352	0.201	**0.143**
PNZ	35.5%	64.7%	**72.3%**
Dice	28.1%	72.5%	**76.1%**

TABLE III
QUANTITATIVE RESULTS (MEAN) OF BIG-SOURCE RECONSTRUCTION IN VALIDATION SET

Method	Tikhonov-L2	IPS	GCN-RC
BCE(mm)	0.372	0.237	**0.151**
PNZ	40.1%	60.7%	**68.3%**
Dice	34.3%	69.8%	**74.4%**

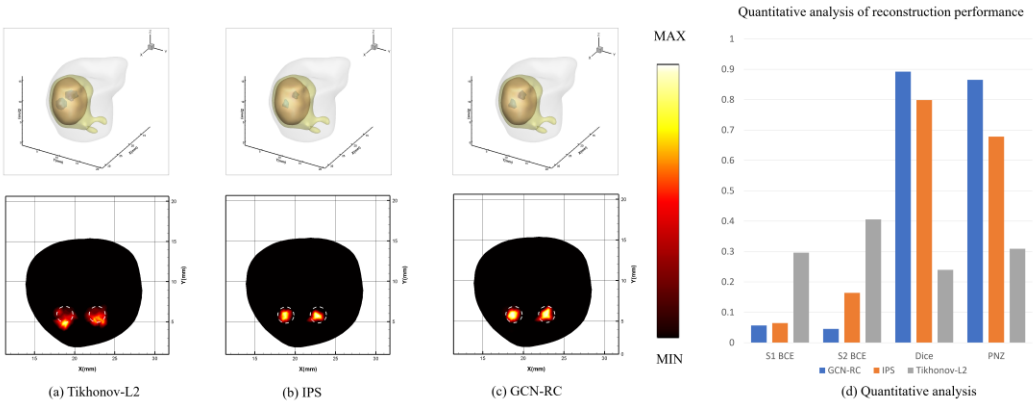

Fig. 3 The qualitative and quantitative analysis of Tikhonov-L2, IPS and GCN-RC reconstruction performance in dual-source reconstruction.

Furthermore, we implemented our method on orthotopic glioma bearing mice to validate the reconstruction performance on real condition. The orthotopic glioma mouse models were established following the protocols of *Meng*[18], and 200 μL orthotopic glioma targeting Tf-IRDye800 fluorescence probe were injected into the mice through tail vein. We utilized an 820±25 nm bandpass filter to collect the emitted light under continuous wave excitation at 750 nm to obtain FMI images of mice. Meanwhile we also collected CT images of mice to get structure information based on the multimodal imaging system. MRI imaging was performed to have orthotopic glioma information in mice, and H&E images of mice was also performed as the gold standard of probe distribution.

As shown in **Fig. 4**, we used MRI-H&E fused images as the gold standard of probe distribution. The reconstruction results of Tikhonov-L2 method were over-smooth and have difficulties in locating the source. The reconstruction results of IPS method appear over-sparse. In contrast, our GCN-RC network can achieve more accurate source localization and morphological reconstruction. In general, *in vivo* experiment potentially highlighted the pre-clinical application of GCN-RC network on FMT reconstruction.

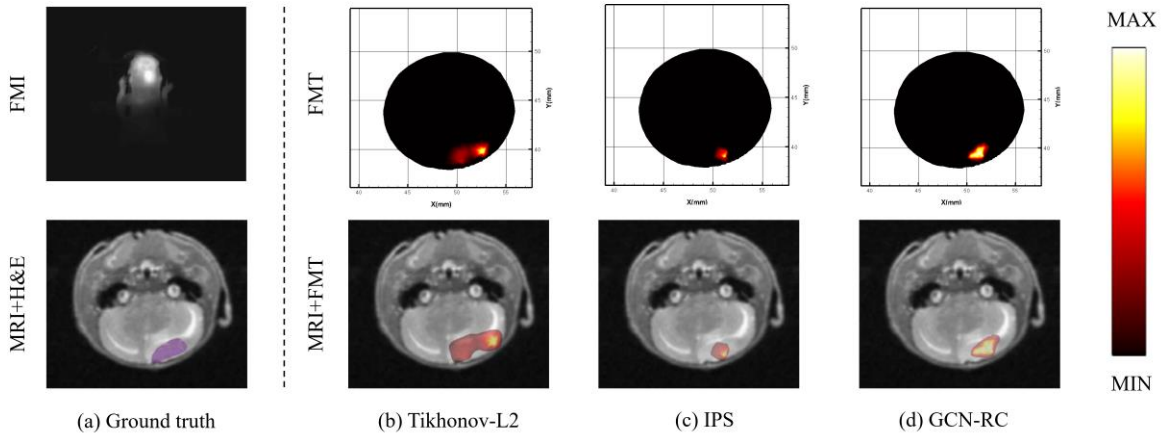

Fig. 4 *In vivo* FMT reconstruction of orthotopic glioma bearing mice. (a) FMI and MRI-H&E fused images. (b)-(d)2D transverse sections of FMT and FMT-MRI fused images obtained using three methods.

4. CONCLUSIONS

In this work, we propose a new FMT reconstruction method based on graph convolution networks. To solve the problem of over-sparse reconstruction by IPS method, we use residual learning and graph convolutional networks to fine-tunes the coarse reconstruction results of IPS. Simulation experiments demonstrated the enhanced performance on reconstruction accuracy and morphological similarity of GCN-RC than IPS and Tikhonov-L2. Moreover, *in vivo* experiments also demonstrated that GCN-RC network can achieve more accurate source localization and morphological reconstruction on FMT reconstruction. Our method is promising to be applied to preclinical and clinical applications in cancer diagnosis and treatment.

5. ACKNOWLEDGEMENTS

This work was supported by Ministry of Science and Technology of China under Grant No. 2017YFA0205; National Natural Science Foundation of China under Grant Nos. 81871514, 81227901, 81470083, 91859119, 61671449, 81527805, 61901472; National Public Welfare Basic Scientific Research Program of Chinese Academy of Medical Sciences under Grant No.2018PT32003, 2017PT32004, National Key R&D Program of China under Grant Nos. 2018YFC0910602, 2017YFA0205200, 2017YFA0700401, 2016YFA0100902, 2016YFC0103702. National Natural Science Foundation of Shaanxi Province under Grant No.2019JM-459.

REFERENCES

[1] M. Koch, P. Symvoulidis, and V. Ntziachristos, "Tackling standardization in fluorescence molecular imaging," *Nat Photonics* **12**(9), 505-515 (2018).
[2] R. Weissleder et al., "In vivo imaging of tumors with protease-activated near-infrared fluorescent probes," *Nat Biotechnol* **17**(4), 375-378 (1999).
[3] Y. An et al., "Application of machine learning method in optical molecular imaging: a review," *Sci China Inform Sci* **63**(1), (2020).
[4] J. Z. Ye et al., "Reconstruction of fluorescence molecular tomography via a nonmonotone spectral projected gradient pursuit method," *J Biomed Opt* **19**(12), (2014).
[5] L. Li et al., "Fluorescence Molecular Imaging and Tomography of Matrix Metalloproteinase-Activatable Near-Infrared Fluorescence Probe and Image-Guided Orthotopic Glioma Resection," *Mol Imaging Biol* **20**(6), 930-939 (2018).

[6] L. Li et al., "Prediction of the anti-glioma therapeutic effects of temozolomide through in vivo molecular imaging of MMP expression," *Biomed Opt Express* **9**(7), 3193-3207 (2018).
[7] Y. An et al., "A Novel Region Reconstruction Method for Fluorescence Molecular Tomography," *IEEE T Bio-Med Eng* **62**(7), 1818-1826 (2015).
[8] X. Cao et al., "An adaptive Tikhonov regularization method for fluorescence molecular tomography," *Med Biol Eng Comput* **51**(8), 849-858 (2013).
[9] Y. Gao et al., "Bioluminescence Tomography Based on Gaussian Weighted Laplace Prior Regularization for In Vivo Morphological Imaging of Glioma," *IEEE T Med Imaging* **36**(11), 2343-2354 (2017).
[10] J. Z. Ye et al., "Sparse Reconstruction of Fluorescence Molecular Tomography Using Variable Splitting and Alternating Direction Scheme," *Mol Imaging Biol* **20**(1), 37-46 (2018).
[11] H. F. Wang et al., "A Novel Adaptive Parameter Search Elastic Net Method for Fluorescent Molecular Tomography," *IEEE T Med Imaging* **40**(5), 1484-1498 (2021).
[12] Y. Gao et al., "Non model-based bioluminescence tomography using a machine-learning reconstruction strategy," *Optica* **5**(11), 1451-1454 (2018).
[13] H. Meng et al., "K-Nearest Neighbor Based Locally Connected Network for Fast Morphological Reconstruction in Fluorescence Molecular Tomography," *IEEE T Med Imaging* **39**(10), 3019-3028 (2020).
[14] T. N. Kipf, and M. J. a. p. a. Welling, "Semi-supervised classification with graph convolutional networks," (2016).
[15] J. W. Shi et al., "Fluorescence molecular tomography reconstruction via discrete cosine transform-based regularization," *J Biomed Opt* **20**(5), (2015).
[16] S. Bartel, and A. H. Hielscher, "Monte Carlo simulations of the diffuse backscattering Mueller matrix for highly scattering media," *Appl Optics* **39**(10), 1580-1588 (2000).
[17] S. H. Ren et al., "Molecular Optical Simulation Environment (MOSE): A Platform for the Simulation of Light Propagation in Turbid Media," *Plos One* **8**(4), (2013).
[18] H. Meng et al., "Adaptive Gaussian Weighted Laplace Prior Regularization Enables Accurate Morphological Reconstruction in Fluorescence Molecular Tomography," *IEEE T Med Imaging* **38**(12), 2726-2734 (2019).